


Numerical and experimental study on knocking combustion in turbocharged direct-injection engines for a wide range of operating conditions

International J of Engine Research
2023, Vol. 24(2) 652–671
© IMechE 2021
Article reuse guidelines:
sagepub.com/journals-permissions
DOI: 10.1177/14680874211060188
journals.sagepub.com/home/fer


Magnus Kircher¹ , Emmeram Meindl² and Christian Hasse¹ 

Abstract

A combined experimental and numerical study is conducted on knocking combustion in turbocharged direct-injection spark-ignition engines. The experimental study is based on parameter variations in the intake-manifold temperature and pressure, as well as the air-fuel equivalence ratio. The transition between knocking and non-knocking operating conditions is studied by conducting a spark timing sweep for each operating parameter. By correlating combustion and global knock quantities, the global knock trends of the mean cycles are identified. Further insight is gained by a detailed analysis based on single cycles. The extensive experimental data is then used as an input to support numerical investigations. Based on 0D knock modeling, the global knock trends are investigated for all operation points. Taking into consideration the influence of nitric oxide on auto-ignition significantly improves the knock model prediction. Additionally, the origin of the observed cyclic variability of knock is investigated. The crank angle at knock onset in 1000 consecutive single cycles is determined using a multi-cycle 0D knock simulation based on detailed single-cycle experimental data. The overall trend is captured well by the simulation, while fluctuations are underpredicted. As one potential reason for the remaining differences of the 0D model predictions local phenomena are investigated. Therefore, 3D CFD simulations of selected operating points are performed to explore local inhomogeneities in the mixture fraction and temperature. The previously developed generalized Knock Integral Method (gKIM), which considers the detailed kinetics and turbulence-chemistry interaction of an ignition progress variable, is improved and applied. The determined influence of spark timing on the mean crank angle at knock onset agrees well with experimental data. In addition, spatially resolved information on the expected position of auto-ignition is analyzed to investigate causes of knocking combustion.

Keywords

Engine, spark-ignition, auto-ignition, knock, knock integral method

Date received: 3 August 2021; accepted: 27 October 2021

Introduction

Knocking combustion in spark-ignited engines is a common irregular combustion phenomenon and can lead to high peak cylinder pressures, pressure gradients, and pressure oscillations. The consequences of these irregularities can include major forms of engine damage. Hence, knock is still a crucial aspect of engine and combustion process development.¹ A recent review can be found in Wang et al.² Different theories have been developed to explain the origin of knock. Ricardo³ proposed auto-ignition theory, which states that engine knock originates in spontaneous auto-ignition processes in the unburned gas ahead of the propagating flame front, which provoke pressure and shock waves. The original detonation theory describes engine knock

as originating in an accelerated primary flame without auto-ignition processes in the unburned gas.⁴ The flame accelerates to sonic velocity and consumes the end gas at a much higher rate than at normal flame speeds. Miller⁵ proposed a combination of detonation theory and auto-ignition theory. This theory is based on the assumption that “after-burning” is possible in a volume

¹Institute for Simulation of reactive Thermo-Fluid Systems, Technical University Darmstadt, Darmstadt, Germany

²BMW Munich, Munich, Germany

Corresponding author:

Magnus Kircher, Institute for Simulation of reactive Thermo-Fluid Systems, Technical University Darmstadt, Otto-Berndt-Straße 2, Darmstadt 64287, Germany.
Email: kircher@stfs.tu-darmstadt.de

of gas that has already been burned by the propagating flame or that has reacted due to auto-ignition. König et al.⁶ showed that the reaction propagation originating from exothermic centers depends not only on the temperature and pressure, but also on the size, distribution, and properties of the exothermic centers. Spicher et al.⁷ investigated knocking combustion in a single-cylinder spark-ignition engine and showed that knock was always initiated by auto-ignition in the unburned gas, clearly separated from the normal flame front. The occurrence of knock and its intensity strongly depend on the mode of propagation following the initial auto-ignition. Following the approach developed by Zeldovich,⁸ and König et al.⁶ introduced three modes of propagation originating from exothermic centers. Based on these findings, Bradley et al.⁹ proposed a theory that is able to classify the mode of auto-ignitive propagation using two dimensionless parameters. Light and moderate knock behave in a deflagrative mode, whereas strong knock seems to be characterized by the transition to developing detonations. In the case of super-knock, several studies have indicated that this most damaging knock mode is caused by detonations.^{10–14} In principle, such local effects can be well studied by multidimensional CFD simulations. While most and even very recent studies used RANS approaches,^{15–18} there is an increasing number of LES studies.^{19–23} With the help of LES, Robert et al.²¹ showed that the intensity of the pressure oscillations depends primarily on the amount of auto-ignited mass. These results may only be explained by a knock theory that combines the auto-ignition of hot-spots with the transition to and the occurrence of detonations, suggesting that:

- Knock is always preceded by auto-ignitions in the unburned mixture.
- Under certain conditions, auto-ignition can lead to knock.
- In the case of light and moderate knock, the pressure wave from the initial auto-ignition is immediately separated from the reaction front. The knock intensity mainly depends on the auto-ignited mass and the reaction front behaves in a deflagrative mode.

The scope of this work is to investigate knocking combustion in turbocharged direct-injection spark-ignition engines both experimentally and numerically. An experimental study based on systemic parameter variations is performed focusing on the transition between knocking and non-knocking operating conditions. The experimental data is used to determine global knock trends. Further, single cycles are analyzed in detail. Based on that, numerical models for the analysis and prediction of knock are applied. The intrinsic model limitations are discussed, as well as implemented improvements. With 0D knock modeling the global

Table 1. Engine specification.

Specification	Value
Engine type	6-cylinder in-line; gasoline
Combustion process	Homogeneous charge; DISI
Valves per cylinder	4
Displacement volume	2979 cm ³
Bore	84.0 mm
Stroke	89.6 mm
Compression ratio	10.2
Injector position	Central
Type of injector	Multi-hole injector

knock trends are investigated for all operation points. There is a special focus on how the model's prediction quality is affected when nitric oxides are taken into consideration. Investigations are also carried out to determine whether 0D knock modeling is able to predict and thus explain cycle-to-cycle variations in knocking quantities, incorporating the detailed experimental data. Finally, there is an examination of the extent to which 3D CFD methods are able to predict spatial phenomena that cannot be resolved by a 0D model. For that purpose, local effects in the form of inhomogeneities in the mixture fraction or temperature are numerically investigated using 3D CFD simulations for selected operating points. The generalized Knock Integral Method (gKIM)¹⁵ is improved and applied to predict auto-ignition. Detailed kinetics and turbulence-chemistry interaction are incorporated to obtain spatially resolved information on the expected auto-ignition position.

The remainder of this paper is structured as follows. First, the experimental setup and the post-processing strategy are presented. Next, the 0D modeling approaches are discussed and the model used in this work to simulate knocking combustion is described. The CFD setup is introduced, 3D knock modeling strategies are presented and the modifications to the generalized Knock Integral Method are explained. The results are discussed in the same order: first the experimental investigations, followed by 0D numerical analysis and concluding with a discussion of the 3D CFD simulations performed. Finally, the main findings are summarized and an outlook identifying improvement strategies is given.

Experimental setup and choice of operating parameters

The experimental investigations are carried out on a turbocharged six-cylinder BMW engine with direct injection, Valvetronic, and homogeneous charge combustion. All operating points are close to full load. Hence, the intake valve lift is set to its maximum value of 9.9 mm. All experiments are performed with RON98 gasoline. The engine specifications are summarized in Table 1.

Table 2. Summary of testing program.

Engine speed	λ [-] 0.05 steps	T_{int} [°C] 5°C steps	p_{int} [mbar] 100 mbar steps
2000 rpm	0.80–1.00	40–60	1780–2180
5000 rpm	0.75–0.90	40–60	1680–1980

Table 3. Reference spark timing sweeps RS1 at 2000 rpm and RS2 at 5000 rpm.

Operating parameter	RS1	RS2
Engine speed [rpm]	2000	5000
Lambda [-]	0.9	0.8
Int.-man. temperature [°C]	50	50
Int.-man. pressure [mbar]	1980	1680
Start of injection [°CA bTDC]	260	260
Rail pressure [bar]	200	200

The test engine is equipped with Kistler piezoelectrical pressure sensors for measuring the cylinder pressure and the intake and exhaust pressures. The cylinder pressure sensor is mounted flush with the combustion chamber dome to reduce acoustic oscillations. In addition, the engine-out CO₂, CO, NO_x, HC, and O₂ emissions are analyzed with a Horiba MEXA-7100HEGR emission measurement system. The testing program particularly targets the stochastic and complex nature of engine knock. The impact of the air-fuel equivalence ratio λ , intake-manifold temperature T_{int} , and intake-manifold pressure p_{int} on engine knock is investigated at engine speeds of 2000 and 5000 rpm (cf. Table 2). All operation points are close to full-load. The parameter ranges aim to reproduce realistic engine conditions of knocking operation.

To study the transition between knocking and non-knocking operating conditions, a spark timing sweep is conducted for each operating parameter. With 7–18 spark timings per sweep, this results in almost 300 operating points. The air mass flow rate is kept constant for all sweeps (except for the intake-manifold pressure sweep) by adjusting the boost pressure. This particular setting makes it possible to obtain a comparable cylinder mass, charge motion and turbulence during the intake stroke. In total, 1000 single cycles are recorded for each operating point.

For each engine speed one spark timing sweep is conducted for all operating parameter variations as a reference point (cf. Table 3). The reference sweep RS1 at 2000 rpm is studied in detail throughout this work. If not stated otherwise, parameter variations correspond to this base point.

Analysis of experimental engine results

The main experimental results are the measured pressure signals, which can be used to obtain the burn rate,

wall heat losses, cylinder charge composition (fuel, air, residual gas) and thermodynamic quantities. In this work, *Three Pressure Analysis* (TPA) is used, as incorporated in the commercial engine cycle simulation tool *GT-POWER*. The crank angle at which 50% of the cylinder mass is burned (MFB50%) is derived from the burn rate.

Looking more specifically at knocking combustion, the most important global knock quantities are the crank angle at knock onset (CAKO), the knock amplitude (KA), and the frequency of knock occurrence (FKO), respectively. All of these quantities can be determined by evaluating the filtered cylinder pressure signal.^{24–30} The characteristically high pressure oscillations of knock can be extracted by applying a zero-phase high-pass filter. The frequency pass of 4 kHz proves to be a good compromise between filtering out undesired noise frequencies and preserving the typical knock frequencies above 6 kHz. According to Schüle et al.,²⁹ a cycle is determined as knocking, if the filtered signal exceeds an engine speed dependent threshold. A threshold of 1.2 bar at 2000 rpm and 3.0 bar at 5000 rpm is chosen. The CAKO is defined as the zero-crossing before the exceedance of this threshold. KA is the maximum of the filtered cylinder pressure.

The mean CAKO and KA are determined from an ensemble average of the knocking cycles:

$$CAKO = \frac{\sum_{i=1}^{N_{cycle}} CAKO_i}{N_{knock}} \quad (1)$$

$$KA = \frac{\sum_{i=1}^{N_{cycle}} KA_i}{N_{knock}}, \quad (2)$$

where $CAKO_i = 0$ and $KA_i = 0$ if i is a non-knocking cycle.

The total number of knocking cycles is denoted by N_{knock} . The frequency of knock occurrence may then be written as

$$FKO = \frac{N_{knock}}{N_{cycle}}. \quad (3)$$

Besides the mean MFB50% of all cycles, a mean MFB50% of the knocking cycles can be determined by

$$MFB50\%_{knock} = \frac{\sum_{i=1}^{N_{cycle}} MFB50\%_i}{N_{knock}}. \quad (4)$$

Again $MFB50\%_i = 0$ if i is a non-knocking cycle.

Simulation of knocking combustion

In this work, we use both 0D and 3D CFD approaches to study knocking combustion and to compare the simulations to experimental results. While 0D models require much less computational time compared to 3D CFD approaches, they cannot resolve local phenomena such as temperature or mixture inhomogeneities. One particular advantage, which is also extensively used here, is that a large number of cycles can be simulated to study cyclic variations. In contrast, 3D CFD knock models are particularly suited for a detailed investigation of how spatial inhomogeneity and the turbulent flame propagation influence the formation and location of critical areas where auto-ignition is likely to occur. In the following, we describe the 0D and the 3D modeling approaches separately.

0D knock modeling approach

In this work we use a 0D knock model coupled with a 1D engine cycle simulation tools. The gas dynamics in the intake and exhaust system are captured by solving one-dimensional conservation equations. The cylinder is assumed to consist of two zones, unburned and burned mixture. The mixture composition and temperature are assumed to be homogeneous in each zone.

The capability of 0D knock models to predict the time of knock onset and the knock intensity has been demonstrated in numerous publications.^{24,31–35}

Two approaches widely used to predict knock are (semi-)empirical correlations or the direct modeling of auto-ignition in the unburned zone. The knock integral method (KIM) is a semi-empirical model introduced by Livengood and Wu³⁶ based on the assumption that the chemical state of an auto-igniting gas can be represented by one species. Auto-ignition takes place at the time t_k when the concentration of this global species $[x]$ reaches a critical value $[x_c]$. The history of the reaction and the buildup of radicals are taken into account by the temporal integration of the rate of change of the concentration of this global species. To make it possible to solve the equation, Livengood and Wu proposed a functional linear relationship between the rate of change and the ignition delay time τ :

$$\left(\frac{[x]}{[x_c]}\right)_{t_k} = \int_{t=0}^{t_k} \frac{d}{dt} \left(\frac{[x]}{[x_c]}\right) dt = \int_{t=0}^{t_k} \frac{1}{\tau} dt = 1. \quad (5)$$

A more detailed approach is based on direct modeling of the chemical kinetics. Complex chemical reaction mechanisms are used to predict the mass fraction of each species involved. As will be shown below, in this study we use detailed kinetics. This makes it possible to study effects such as the reduction of the auto-ignition delay time by NO. Further, the same detailed kinetics will be used to tabulate the auto-ignition delay times τ_i for the generalized knock integral method (gKIM) used in the 3D CFD.

Implementation of 0D knock model

As mentioned above, a two-zone model is used. In each zone, the conservation equations for mass, energy, and species and the equation of state are solved by the multi-purpose chemistry solver *ProEngine* incorporating chemical kinetics.^{15,37} The iso-octane reaction mechanism consisting of 222 species and 1506 reactions (cf. Mechanism B by Linse³⁷) is extended by NO reactions taken from.⁵⁴

The mass exchange between the two zones, the total volume of the reactor network and the wall heat losses of both zones are taken into account by coupling with *GT-POWER*. During the simulation run, the required variables are transferred from *GT-POWER* to *ProEngine* at each time step and the system of differential equations is solved.

The unburned zone is assumed to initially consist of the fresh charge and internal residual gas. The trapped fuel and air mass and the residual gas mass fraction are determined by the *GT-POWER* gas exchange simulations. The composition of the residual gas is calculated with *ProEngine*. The total wall heat losses determined by *GT-POWER* are distributed to the burned and unburned zone by their respective volume fraction.

When determining the crank angle at knock onset (CAKO), it is assumed that the time of auto-ignition is an adequate approximation. The auto-ignition of the unburned zone leads to a rapid exothermic energy release associated with a steep temperature and pressure rise. The CAKO is defined as the crank angle at which the unburned temperature exceeds a specified threshold.

3D CFD modeling approach

The 3D-CFD RANS simulations are particularly used to study the global knock trends of numerous engine operating points. In addition, local mixture, and temperature information is used to investigate the tendency to auto-ignition in different areas of the cylinder.

3D CFD setup and boundary conditions

CFD solver and modeling approach. The commercial code ANSYS CFX is used to perform the 3D CFD simulations. Turbulence is solved for by the standard $k - \varepsilon$ turbulence model combined with the Kato and Launder³⁸ limiter to limit the production of turbulent kinetic energy in stagnation regions. Turbulent premixed flame propagation is modeled using the G-Equation model, which is a flamelet based level-set approach that has been successfully applied to predict premixed turbulent combustion in SI engines in several scientific works.^{37,39,40} The reaction progress is described by the Favre average of the progress variable \tilde{c} defined by a tracer species.

The meshing process is automatically controlled by ANSYS CFX Pistongrid. A certain mesh is

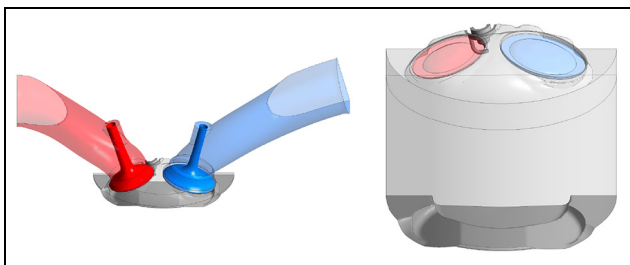


Figure 1. Computational domain: gas exchange (left), compression/combustion (right).

continuously moved until the quality is below the user prescribed threshold. Then, the generation of a new mesh is triggered and the results of the previous run are mapped onto the current before simulation the continues. Time step control is achieved by limiting the maximum crank angle step $\Delta\alpha$ to 0.25°CA generally and to 0.1°CA for the more critical phases of valve overlap, injection and combustion.

The engine geometry is symmetrical with respect to the tumble plane. Symmetrical valve lifts result in swirl-free operation. The six-hole injector is aligned with the symmetry plane of the engine. Due to this symmetry, only a 180° mesh is used for the RANS simulations. The meshes use continuous prism elements to resolve the boundary layer and tetrahedral cells in the remaining domain. The mesh resolution is increased in the intake valve gap and the direct vicinity. This strategy results in a total number of 500,000 cells when both valves are closed and up to approximately 2.7 million when the intake valve is open. Figure 1 shows the computational domain during the valve overlap phase and when both valves are closed. The exhaust side is shown in red, the intake side is highlighted in blue.

To ensure a good numerical representation of the entire engine cycle, the following key aspects are incorporated:

- **Gas exchange:** Boundary and initial conditions are determined by 1D gas exchange simulations. The pressure and temperature histories are specified at the exhaust port outlet. At the inlet of the intake port the mass flow rate and temperature history are imposed.
- **Fuel injection:** The applied injection model is based on the specification of the initial droplet velocity, size, and distribution at the nozzle outlet. The particle properties correspond to the state after secondary breakup, that is, no breakup model is used. Experimental spray visualizations for different thermodynamic conditions are used to calibrate the model parameters (cf. Stach et al.⁴¹). Mass transfer from the liquid to the gas phase is accounted for by a suitable evaporation model.
- **Wall temperatures:** A detailed wall temperature distribution is obtained by an iterative 3D conjugate heat transfer (CHT) simulation of the in-cylinder

flow, structure and coolant flow for selected operating points. This detailed distribution is scaled based on the area-averaged wall temperatures predicted by a 1D engine cycle simulation for all other points.

3D knock modeling approaches. Common CFD approaches for knock can be divided into two major groups:

- Prediction of the onset of auto-ignition by a pseudo precursor
- Direct modeling of auto-ignition by detailed chemical kinetics

The precursor models are based on the assumption that the chemical state of an auto-igniting gas can be represented by one reactive scalar. A transport equation for the precursor is solved in order to take into account the interaction of transport and chemistry.

Following the discussion above, the knock integral method (KIM)³⁶ provides a suitable description of the chemical source term of the precursor:

$$\tilde{\omega}_{Y_p} = \frac{1}{\tilde{\tau}}. \quad (6)$$

Auto-ignition occurs when the precursor mass fraction reaches a value of 1. Typically, the effect of the turbulence-chemistry interaction is neglected. Hence, the chemical ignition delay time $\tilde{\tau}$ is determined using the Favre-averaged local quantities, that is, chemical composition and temperature, in each cell without taking into account their fluctuations, which may result in a considerable error.

Precursor models have been widely used to predict auto-ignition. Ignition delay times can be calculated by an empirical correlation as done by Lafossas et al.⁴² and Kleemann et al.⁴³ Both reduced reaction mechanisms (Teraji et al.⁴⁴ and Christiner et al.^{28,45}) and complex reaction mechanisms (Jaworski et al.⁴⁶) have been used to compute and tabulate ignition delay times for varying conditions.

One disadvantage of the precursor model is the underlying assumptions for the source term modeling. An alternative is the direct modeling of the auto-ignition process, where simplified kinetics are, however, usually employed. These can be either reduced versions of detailed mechanisms^{47–49} or multi-step mechanisms with pseudo-species such as the Shell model.^{50,51}

In general, it should be noted that the use of RANS modeling inevitably leads to a loss of statistical information. This can be partially compensated for; for example D'Adamo et al.¹⁶ considered turbulence-induced variations in the knock onset. Additional transport equations for the variance in the mixture fraction and enthalpy are solved. Their joint effect is taken into account by using a multivariate Gaussian distribution to calculate the Favre-averaged chemical source term of the knock precursor and its variance.

The introduction of statistical information makes it possible to provide a quantitative estimate of the knock probability. Similarly, the generalized knock integral method (gKIM) used in this work uses local distributions of at least the temperature and the mixture fraction to determine the source of the ignition progress variable. Thus, it also takes into account turbulence-chemistry interaction and the stochastic nature of knock. The integration of an improved version of gKIM into a 3D CFD framework is described next.

Improved generalized knock integral method. The following section briefly describes the gKIM including some improvements made for this work, and the coupling to the 3D CFD solver. The generalized knock integral method (gKIM) proposed by Linse et al.¹⁵ is chosen as the starting point. A transport equation for an ignition progress variable \tilde{c}_I is solved. One distinctive feature is that the chemical source term takes into account both auto-ignition and regular combustion, that is, flame propagation.¹⁵ This ensure that the ignition progress variable equals zero for $\tilde{c} = 1$. However, the formulation of the chemical source is sensitive to numerical inaccuracies.

Thus, an alternative formulation of the gKIM is proposed. A transport equation for the Favre-averaged ignition progress conditioned on the unburned $\tilde{c}_{I,u}$ is solved instead of the transport equation for \tilde{c}_I as in Linse et al.¹⁵:

$$\frac{\partial(\bar{\rho}\tilde{c}_{I,u})}{\partial t} + \frac{\partial}{\partial x_i}(\bar{\rho}\tilde{u}_i\tilde{c}_{I,u}) = \frac{\partial}{\partial x_i} \left(\frac{\mu_t}{Sc_{t,c_{I,u}}} \frac{\partial \tilde{c}_{I,u}}{\partial x_i} \right) + \bar{\rho}\tilde{\omega}_{c_{I,u}}. \quad (7)$$

Assuming that auto-ignition cannot occur in the burned mixture, the ignition progress \tilde{c}_I can then be expressed by a linear combination of the reaction progress \tilde{c} and the conditional ignition progress $\tilde{c}_{I,u}$:

$$\tilde{c}_I = (1 - \tilde{c}) \cdot \tilde{c}_{I,u}. \quad (8)$$

Further, an equation for the variance of the ignition progress variable c''^2 is solved.

$$\frac{\partial(\bar{\rho}c''^2)}{\partial t} + \frac{\partial}{\partial x_i}(\bar{\rho}\tilde{u}_i\tilde{c}_I''^2) = \frac{\partial}{\partial x_i} \left(\frac{\mu_t}{Sc_{t,c_I}} \frac{\partial c_I''^2}{\partial x_i} \right) + 2 \frac{\mu_t}{Sc_{t,c_I}} \frac{\partial \tilde{c}_I}{\partial x_i} \frac{\partial \tilde{c}_I}{\partial x_i} - 2\bar{\rho} \frac{\tilde{c}_I}{k} \tilde{c}_I''^2 + 2\bar{\rho}\tilde{c}''\tilde{\omega}_{c_I}. \quad (9)$$

The turbulent Schmidt number Sc_{t,c_I} is set to 0.9 and molecular diffusion terms are neglected.

The Favre-averaged chemical source terms are derived by applying a presumed PDF approach. The sample space variables of the joint PDF $P(\theta, \theta_I, \phi)$ are summarized in Table 4.

Table 4. Sample space variables of the joint PDF. The scalars Ψ_i are: temperature T , mixture fraction Z , pressure p , and residual gas mass fraction Y_{EGR} .

Variable	Sample space variable
c	θ
c_I	θ_I
$\Psi_1 = T$	ϕ_1
$\Psi_2 = Z$	ϕ_2
$\Psi_3 = p$	ϕ_3
$\Psi_4 = Y_{EGR}$	ϕ_4

Table 5. Presumed PDF of the reactive/non-reactive scalars.

Scalar	PDF shape
$\tilde{P}(\phi_1 _{c=0})$	Clipped Gaussian PDF
$\tilde{P}(\phi_2 _{c=0})$	Beta PDF
$\tilde{P}(\phi_3 _{c=0})$	Delta function
$\tilde{P}(\phi_4 _{c=0})$	Delta function

As in our earlier work, the following assumptions are used:

- Only fully burned and unburned conditions appear, which reduces the PDF of the reaction progress $\tilde{P}(\theta)$ to two delta functions.
- The reactive/non-reactive scalars Ψ are statistically independent.

Finally, the Favre-averaged source terms can be expressed as:

$$\tilde{\omega}_{c_{I,u}} = \tilde{\tau}^{-1}|_{c=0}. \quad (10)$$

$$\tilde{c}''\tilde{\omega}_{c_I} = \tilde{c}_I\tilde{\tau}^{-1}|_{c=0} - \tilde{c}_I\tilde{c}_I|_{c=0}\tilde{\omega}_{c_I} - \tilde{c}_I \cdot \tilde{\omega}_{c_I}. \quad (11)$$

The Favre-averaged inverse chemical ignition delay time conditioned on the unburned mixture $c = 0$ is described by:

$$\tilde{\tau}^{-1}|_{c=0} = \int_{\phi_{min}}^{\phi_{max}} \tau^{-1}|_{c=0} \cdot \tilde{P}(\phi|_{c=0})d\phi. \quad (12)$$

The PDFs of the scalars Ψ are summarized in Table 5 (cf. Linse et al.¹⁵):

The clipped Gaussian PDF and the beta PDF are uniquely defined by the Favre-average and the variance in the corresponding quantities. The fluctuation intensity $I_{T|_{c=0}}$ of the conditional temperature $T|_{c=0}$ is assumed to equal the fluctuation intensity I_T of the unconditional temperature T .

$$I_T = \frac{\sqrt{T''^2}}{\bar{T}} = \frac{\sqrt{T''^2|_{c=0}}}{\bar{T}|_{c=0}}. \quad (13)$$

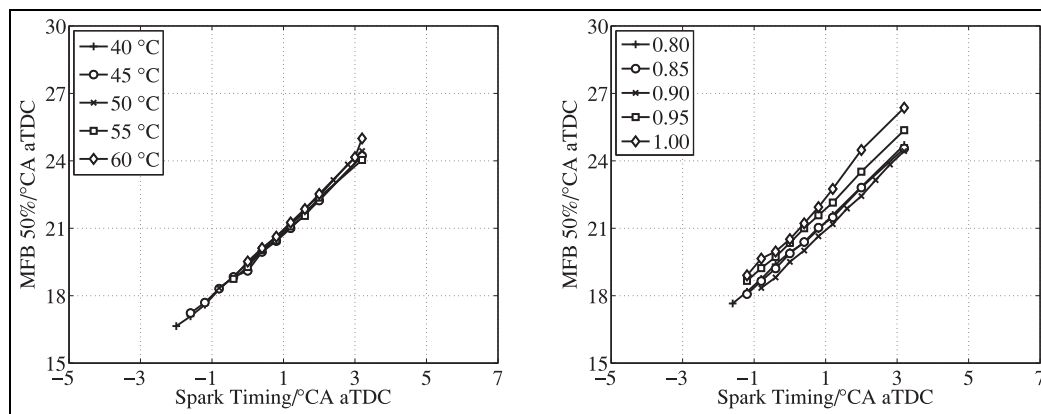


Figure 2. Influence of spark timing and intake-manifold temperature (left) and λ (right) on MFB50% at 2000 rpm.

The variance in the unconditioned temperature \widetilde{T}''^2 and the mixture fraction \widetilde{Z}''^2 are determined by the corresponding transport equations.

The chemical ignition delay times are calculated a priori using the same iso-octane reaction mechanism as in the 0D model. Subsequently the ignition delay times are Favre-averaged, that is, convoluted with the PDF, and tabulated as a function of the pressure, unburned temperature, mixture fraction, residual gas mass fraction, mixture fraction variance, and unburned temperature variance. During the CFD simulation run, the Favre-averaged inverse ignition delay times are determined by linear interpolation of the table values.

The PDF shape of the ignition progress variable is described by a clipped Gaussian PDF with upper and lower limits of 1.0 and 0.0, respectively using the mean and variance of the ignition progress. The ignition probability is defined as:

$$I_p = \text{prob}(c_I > \zeta) = \int_{\theta_I = \zeta}^1 \widetilde{P}(\theta_I; \mathbf{x}, t) d\theta_I. \quad (14)$$

ζ is a user defined lower integration limit. By that means, it is possible to identify a set Ω_{I_p} representing all computational cells that exhibit an ignition probability greater than a user-defined threshold ε :

$$\Omega_{I_p} = \{(x, y, z) \in \mathfrak{R}^3 | I_p(x, y, z) \geq \varepsilon\}. \quad (15)$$

$\zeta = 0.95$ and $\varepsilon = 0.01$ are chosen, as proposed by Linse et al.¹⁵

Based on these cells, the critical mass can be determined:

$$m_{I_p} = \int_{\Omega_{I_p}} \bar{\rho} dV. \quad (16)$$

Experimental results

Knock is investigated experimentally and numerically with 0D and 3D-CFD approaches. The experimental

studies provide a comprehensive data base for analyzing global knock trends as well as for conducting studies on a per-cycle basis. The 0D knock model is used to analyze how nitric oxide affects auto-ignition and whether cyclic variations can be captured with experimental single cycle boundary conditions. Finally, 3D CFD simulations will be used to investigate how spatial inhomogeneities in thermochemical state variables affect the probability of auto-ignition at different locations in the cylinder.

First, the influence of the experimentally operating parameter variations (cf. Table 2) on the combustion is investigated. As expected, earlier spark timings shift the combustion and earlier MFB50% can be observed. Moreover, a faster combustion occurs with earlier spark timings. A modification of the spark timing by -2°CA results in a MFB50% that is approximately 3°CA earlier. In Figure 2 an example of this is shown for the variation in the intake-manifold temperature and λ at 2000 rpm. The variation in the intake-manifold pressure exhibits similar behavior. An earlier MFB50% leads to an increase in the cylinder pressure and end-gas temperature and thus promotes knock. Therefore, the evaluation of knock will be based on MFB50% instead of the spark timing in the following.

Exhaust gas composition and residual gas content

An important parameter for the subsequent analysis is the in-cylinder residual gas mass fraction, which is computed by the pressure trace analysis for the averaged engine cycles (single cycle analysis is discussed later). At 2000 rpm, the residual gas mass fraction is almost constant at 1.25% and only marginally affected by varied operating parameters.

Another important aspect is the engine-out exhaust gas composition, which is hardly affected by variations in the pressure and temperature of the intake manifold and nearly constant over the different spark timings.

For the reference spark timing sweep RS1 (cf. Table 3), the measured emissions are summarized in Table 6.

Table 6. Engine-out emissions for RSI (cf. Table 3).

Species concentration	2000 rpm
CO [Vol-%]	≈3.5
CO ₂ [Vol-%]	≈11.0
NO _x [ppm]	≈1000

Richer mixtures of the testing program (cf. Table 2) show less NO_x emissions while for stoichiometric conditions at 2000 rpm they are at around 3000 ppm.

Global knock trends

Knock can be characterized by a few global quantities such as the mean crank angle at knock onset (CAKO), the mean knock amplitude (KA), and the frequency of knock occurrence (FKO). The following discussion only examines how λ influences operating points with a minimum FKO of 1%.

Figure 3 shows MFB50% or MFB50%_{knock} (cf. Equation 4) influence indicated mean effective pressure (IMEP), FKO, CAKO, and KA, this is illustrated for different values of λ at 2000 rpm. Operation at 5000 rpm shows comparable trends.

- The richest mixtures have the highest IMEP as shown in the upper left plot. This can be explained

by the fact that even at the same MFB50%, the shortest combustion duration and thus the highest efficiency is achieved by mixtures with the largest burning velocity. A 1% reduction in air mass flow rate and the lower burning velocity at stoichiometric operation result in an approximately 1 bar lower IMEP. Higher IMEPs lead to an increase in temperature and pressure in the end-gas and promote knock. Therefore, different IMEPs at the same MFB50% may affect the knock evaluation.

- As expected, and as can be seen in the top right plot, FKO increases with an earlier MFB50%. A higher cylinder pressure and end-gas temperature reduce the chemical auto-ignition delay times and consequently increase the probability of knock. At the same MFB50%, FKO decreases with richer mixtures. Due to the lower ratio of specific heats and the increased cooling associated with the heat of evaporation of the excess fuel, the end-gas temperature decreases and the auto-ignition delay time is extended. The stoichiometric operation does not comply with this trend due to a significantly lower IMEP.
- The bottom left plot shows that earlier MFB50%_{knock} leads to an earlier CAKO. This is due to the shorter ignition delay times. A shift in MFB50%_{knock} by -1.0°CA decreases CAKO by approximately 1.5°CA . At the same MFB50%_{knock},

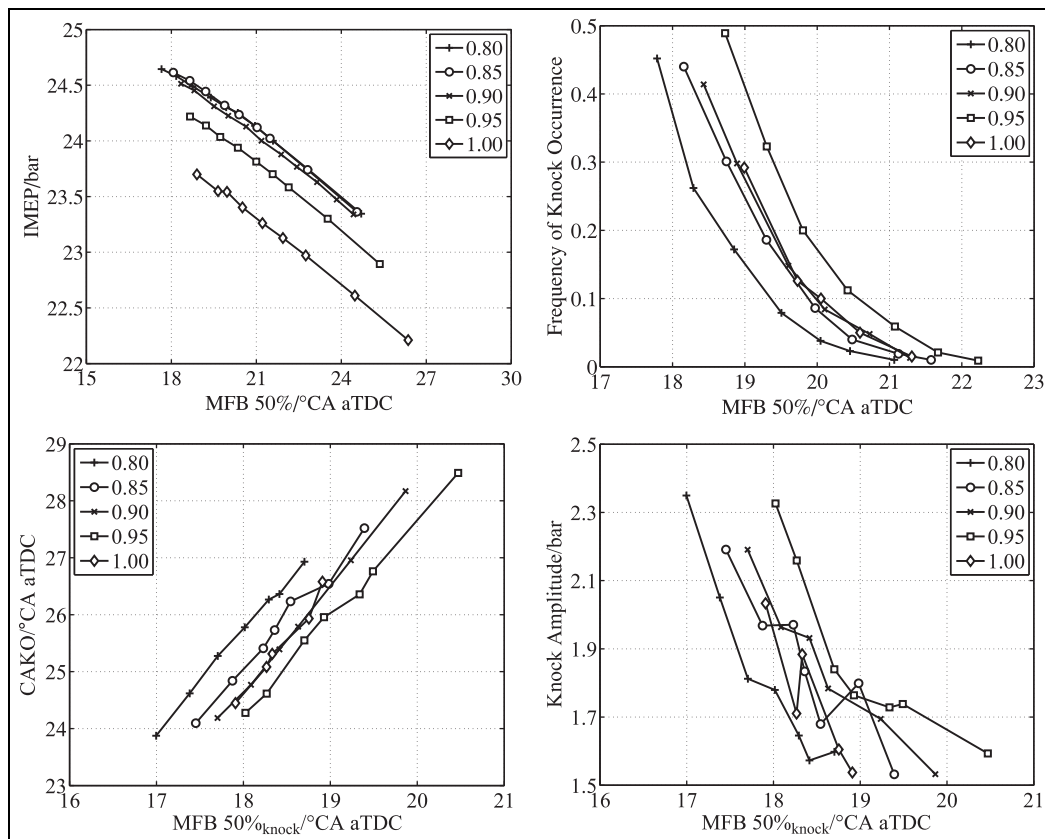


Figure 3. Influence of λ and MFB50% or MFB50%_{knock} on IMEP (top left), FKO (top right), CAKO (bottom left), and KA (bottom right) at 2000 rpm.

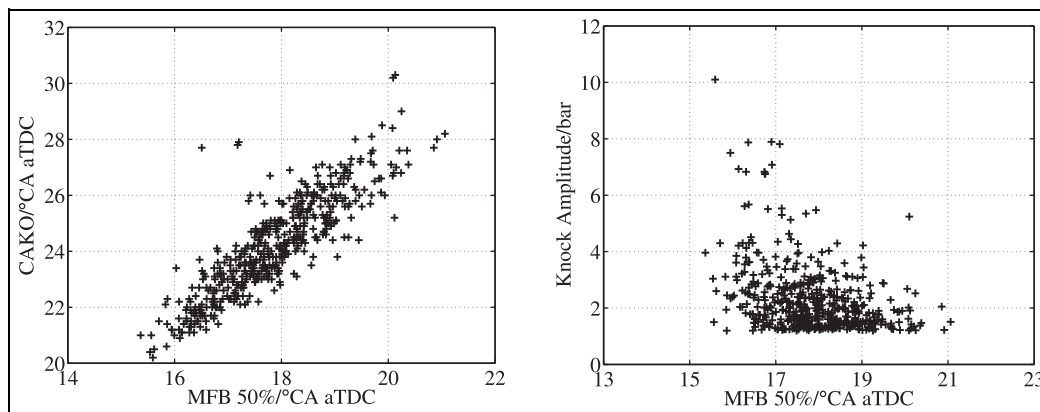


Figure 4. Dependence of CAKO (left) and KA (right) on MFB50%.

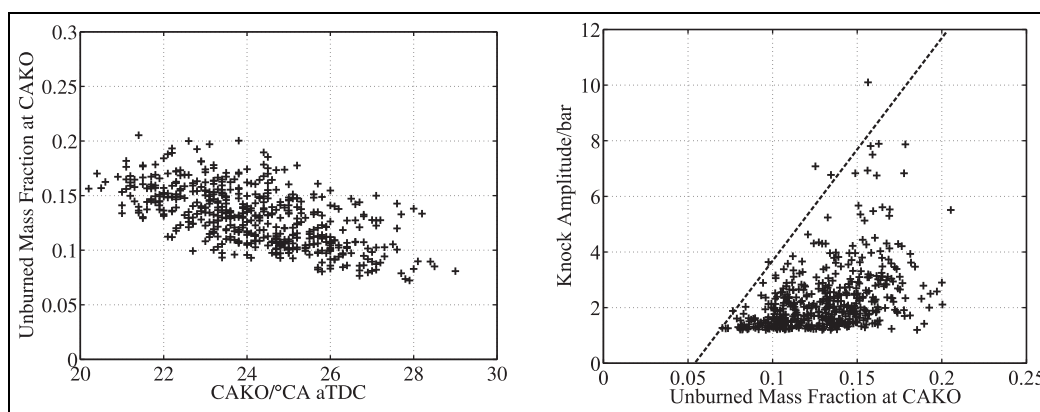


Figure 5. Influence of CAKO on unburned mass fraction at CAKO (left) and dependance of KA on unburned mass fraction at CAKO (right).

later CAKO are achieved with reduced lambda (with the exception of $\lambda = 1.0$ for the same reason as before). The later CAKO of the richer mixtures can be explained by the longer ignition delay time associated with the reduced end-gas temperature

- The bottom right plot shows that an earlier MFB50%_{knock} promotes higher knock amplitudes. This is due to the accelerated auto-ignition reactions. As expected, leaner mixtures tend to result in higher knock amplitudes with the exception already discussed of $\lambda = 1.0$.

Correlations based on single cycle analyses

Knock is a stochastic phenomenon and usually the global trends/statistics are reported. The extensive database in this work allows to study also single cycles. For this purpose, the 1000 individual cycles of the earliest spark timing of the reference operating point at 2000 rpm are analyzed. The unburned temperature and burn rate of each single cycle are obtained by the pressure trace analysis. Cyclic variations in the cylinder pressure and end-gas temperature are caused by cyclic combustion variations. This detailed information

allows to quantify the impact of the single cycle MFB50% on CAKO and KA (cf. Figure 4).

MFB50% has a strong influence on CAKO and the correlation is almost linear as shown in the left plot. An earlier MFB50% promotes earlier CAKO due to the higher cylinder pressure and end-gas temperature. The mean MFB50% of the knocking cycles (17.9°CA aTDC) is considerably earlier than the mean MFB50% of the non-knocking cycles (19.2°CA aTDC). Hence, knock tends to appear in cycles with early MFB50%, which is the expected behavior. However, there is not such a distinct trend for the correlation between KA and MFB50% as shown the right-hand plot. But high knock amplitudes tend to occur at an earlier MFB50%.

The unburned mass fraction at CAKO is a measure for the maximum possible energy release. The left plot in Figure 5 shows that higher unburned mass fractions at CAKO of up to 20% are observed with an earlier CAKO. In the right plot of Figure 5, the correlation between the unburned mass fraction at CAKO and KA is depicted, which can be summarized as follows:

- The same KA appears at very different unburned mass fractions at CAKO. This suggests that only a

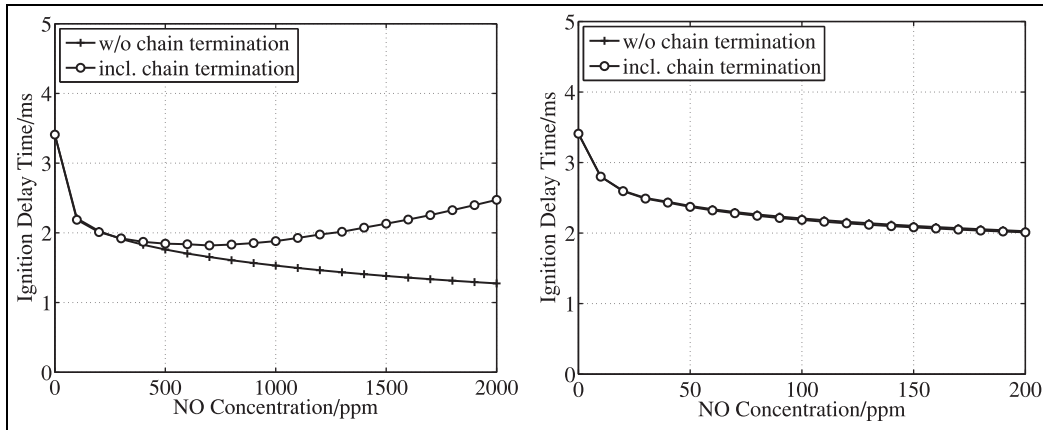


Figure 6. Impact of NO inhibition mechanism (left) and small amounts of NO (right) on ignition delay times.

certain portion of the unburned mixture auto-ignites.

- With a higher KA, the range of unburned mass fractions decreases considerably, which indicates that a higher portion of the unburned mass fraction is consumed by auto-ignition. Moreover, the lower limit of unburned mass fraction at CAKO for a certain KA level increases with a higher KA (indicated by the dashed line). Hence, it can be concluded that higher KAs are caused by a higher auto-ignited mass fraction.

0D knock modeling

These experimental data are used in the following for the 0D and 3D CFD simulations for comparison and further analysis. First, the influence of NO on the ignition delay time is evaluated for the operating points relevant here.

Influence of NO on auto-ignition and knock

The impact of NO on auto-ignition and knock has been studied in numerous publications.^{52–61} NO has been found to significantly reduce ignition delay times and therefore promotes auto-ignition and knock. Using detailed chemistry allows to quantify how NO influences auto-ignition. Here, an adiabatic constant volume reactor is initialized according to full load TDC conditions. The temperature is set to 750 K and the pressure to 40 bar; the mixture is stoichiometric. The fresh mixture is diluted with NO to investigate the influence on the ignition delay time.

As indicated by Figure 6, adding NO to the fresh mixture has a significant influence on the ignition delay time. For high concentrations (left plot) there is a difference in the predicted ignition delay time depending on whether or not NO chain termination reactions are included in the mechanism. However, experimental results at 2000 rpm give a maximum NO concentration

in the unburned mixture of approximately 40 ppm, resulting from a total residual gas fraction of 1.25% and a maximum NO concentration of 3000 ppm. As indicated by the right-hand plot of Figure 6, already this small amount of NO leads to a substantial reduction of approximately 30% in the ignition delay times.

Simulation results – 0D model

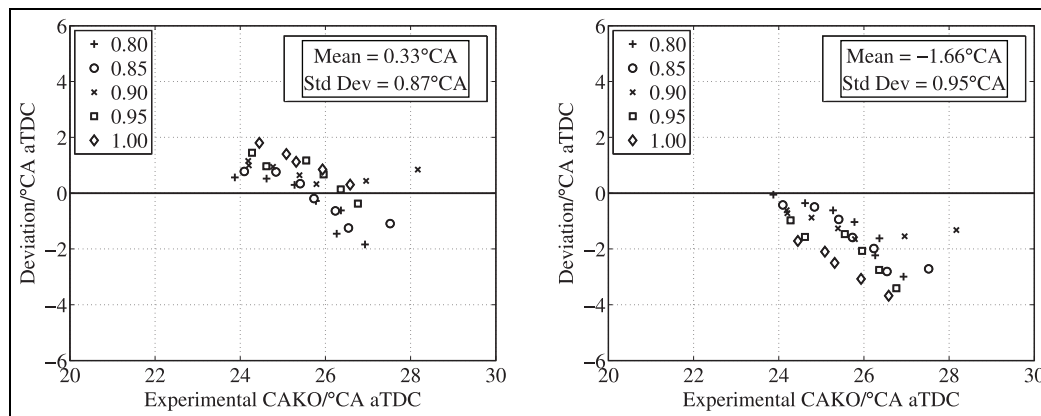
To quantify how NO influences the predicted crank angle at knock onset, 0D knock simulations of the mean engine cycles of all knocking operating points are carried out with and without the presence of NO in the residual gas. The deviation between the simulated and measured mean CAKO is determined as a measure of the model accuracy. In addition, the mean μ_{Δ} and the standard deviation σ_{Δ} of $\Delta = CAKO_{exp} - CAKO_{sim}$ are computed to further characterize the model accuracy. This analysis will be carried out for different operating parameters, μ_{Δ} and σ_{Δ} of the individual spark timing sweeps are determined. Based on Figure 6, the influence of NO is expected to be strongest for the operating points with high NO concentrations. As briefly explained above, NO emissions at the engine outlet are hardly affected by the variation of temperature and pressure in the intake manifold, but are strongly influenced by λ . Thus, the influence of NO on auto-ignition is expected to depend on λ .

Table 7 and Figure 7 summarize the results for μ_{Δ} and σ_{Δ} for the spark timing sweeps for different air-fuel ratios λ at 2000 rpm. It can be clearly seen that a much better agreement between the simulation and the experiment is achieved when NO is taken into account, this holds true both for μ_{Δ} and σ_{Δ} . Further, the difference in μ_{Δ} becomes smaller for richer mixtures as a result of the decreased NO emissions. The same trends are observed for the intake-manifold pressure and temperature variations.

Considering the entire experimental test matrix for 2000 and 5000 rpm, the overall comparison is shown in Table 8. This confirms the observation above that NO

Table 7. λ Variation at 2000 rpm: Influence of NO on μ_{Δ} [$^{\circ}\text{CA}$] and σ_{Δ} [$^{\circ}\text{CA}$].

2000 rpm λ Var.	With NO		Without NO		Difference	
	μ_{Δ}	σ_{Δ}	μ_{Δ}	σ_{Δ}	μ_{Δ}	σ_{Δ}
0.80	-0.40	0.89	-1.27	0.99	0.87	-0.10
0.85	0.19	0.78	-1.57	0.92	1.38	-0.14
0.90	0.76	0.28	-1.14	0.38	1.90	-0.10
0.95	0.67	0.62	-2.04	0.82	2.71	-0.20
1.00	1.10	0.51	-2.61	0.70	3.71	-0.19
All	0.33	0.87	-1.66	0.95	2.00	-0.07

**Figure 7.** Deviation of predicted CAKO including NO (left) versus excluding NO (right). Variation in λ and spark timing at 2000 rpm.**Table 8.** Overall influence of NO inclusion on μ_{Δ} [$^{\circ}\text{CA}$] and σ_{Δ} [$^{\circ}\text{CA}$].

	With NO		Without NO		Difference	
	μ_{Δ}	σ_{Δ}	μ_{Δ}	σ_{Δ}	μ_{Δ}	σ_{Δ}
2000 rpm	0.30	0.74	-1.69	0.81	1.99	-0.07
5000 rpm	0.91	0.82	-3.09	3.35	4.00	-2.53
All	0.56	0.83	-2.29	2.38	2.85	-1.55

must be considered in the simulation. This is remarkable since the residual gas mass fraction only ranges between 1% and 3%, but the predicted knock onset is very sensitive to the presence of NO in the exhaust gases.

It can therefore be concluded that NO should be taken into account in a knock modeling approach based on detailed chemical kinetics. In general, the overall accuracy is remarkable despite the simplifications inherent in the 0D approach. The deviation between the experimental and simulated CAKO is between -1°CA aTDC and $+1^{\circ}\text{CA}$ aTDC for most of the operating points. However, both CAKO and KA fluctuate significantly at the same MFB50%, while knocking and non-knocking cycles also occur. This will be further analyzed in the following sections.

Cycle-to-cycle variations

The single cycle analysis shows significant cycle-to-cycle knock variations even at identical MFB50%. While cycle-to-cycle combustion variations certainly contribute to the knock behavior, additional effects must also play an important role. Therefore, cyclic variations in the cylinder mass, residual gas mass fraction and residual gas composition are investigated and the impact on the predicted crank angle at knock onset is evaluated by applying the 0D knock model.

The cylinder mass and composition are mainly influenced by the intake and exhaust port pressure traces. The 1000 single cycles of the earliest spark timing of the reference spark timing sweep at 2000 rpm (cf. Table 3) are evaluated and the trapped air mass and the residual gas mass fraction is determined using the pressure trace analysis. The results are depicted in Figure 8. The mean of the trapped air mass and residual gas mass fraction of the 1000 single cycles is almost identical to the results for the averaged engine cycle (1046 mg/1.23%). The standard deviation of both variables is very small, indicating that cyclic variations in the cylinder charge mass and residual gas mass fraction are of minor importance.

We showed in the previous section that the composition of the residual gas influences the chemical ignition delay times and hence knock. To better understand the

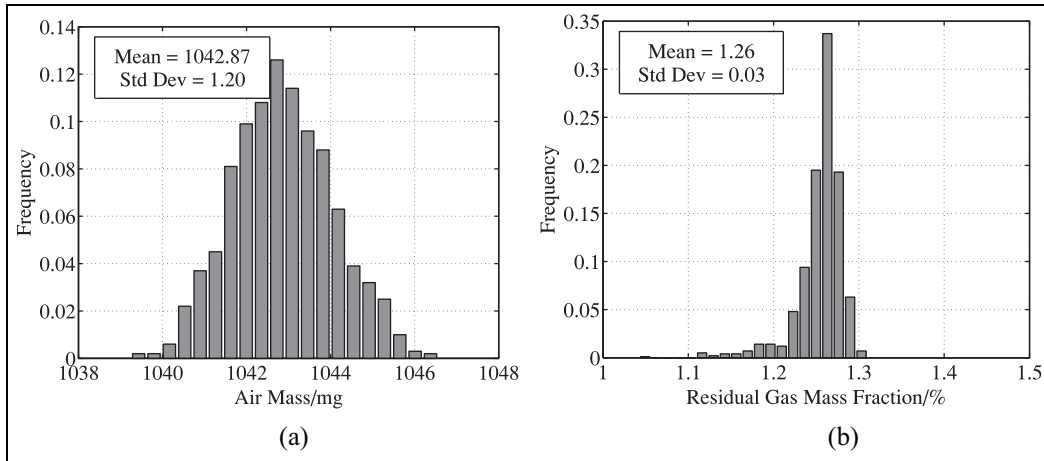


Figure 8. Fluctuation of the cylinder mass (left) and residual gas mass fraction (right): (a) histogram of the trapped air mass, and (b) histogram of the residual gas mass fraction.

effects of cycle-to-cycle variations, the 0D model is used to determine the concentration of residual gas species for 1000 consecutive individual cycles. The measured single cycle intake and exhaust port pressures are imposed and the individual cycle burn rates are determined by means of thermodynamic calculations. Since no information about the injected fuel mass of the individual cycles is available, the same fuel mass is used for each single cycle.

In addition, the modeling approach is applied to the averaged engine cycles and validated against the experimental data from the emission measurement system, which can only provide time-averaged values. The measured and predicted mean CO, CO₂, and NO engine-out emissions of the reference spark timing sweep at 2000 rpm are shown on the left-hand side of Figure 9. The model is able to capture the trend for the different spark timings and can also predict the absolute value of the engine-out emissions with reasonable accuracy.

When the residual gas model is applied to the presented 1000 single cycles, this gives the histograms of the predicted single cycle CO, CO₂, and NO engine-out emissions, which are depicted on the right-hand side of Figure 9. The residual gas species distribution functions are close to the normal distribution. The mean values of the 1000 single cycles match the results of the averaged cycles and only minor fluctuations occur.

Although cyclic variations in trapped air mass, residual gas mass fraction, and residual gas composition are small, given the strong sensitivity of auto-ignition to residual gas mass and composition, the influence of cyclic variability on single-cycle knocking behavior is investigated. The CAKO of the 1000 consecutive single cycles is determined by a multi-cycle knock simulation. The single cycle results are used to initialize the residual gas composition, the experimental intake and exhaust port pressure traces are imposed and the combustion is described by the corresponding burn rates. The

experimental and predicted CAKO of the single cycles are depicted in Figure 10. The overall trend is seen to be captured well by the simulation. However, the model is not able to reproduce the fluctuations of CAKO. At the same MFB50%, the experimental CAKO has a fluctuation range of 2–3°CA, whereas the simulation exhibits a fluctuation range of approximately 1°CA. Hence, cycles with similar burn rates (MFB50%) lead to comparable predicted CAKOs.

Furthermore, the experimental results show that knocking and non-knocking cycles occurred at the same MFB50%. In contrast, the knock model predicts auto-ignition in all cycles with comparable burn rates. This indicates that the 0D model lacks information crucial for the prediction of certain cycles. It is not unexpected that the origin of the cycle-to-cycle variations in CAKO and the occurrence of knocking and non-knocking cycles cannot be fully explained by the 0D model since it is limited to a spatially averaged description of processes. Local effects such as mixture and temperature stratification are not taken into account. Such information can only be provided by 3D simulations which are discussed next.

3D CFD using the generalized Knock Integral Method (gKIM)

Based on the findings above, a selection of operating points are investigated more closely using 3D CFD RANS combustion simulations. In particular, the additional information provided by the presumed PDF approach of the gKIM allows to investigate how temperature and mixture inhomogeneities and the turbulent flame propagation affect the local ignition probability. The following discussion will be focused on the reference spark timing sweep RS1 at 2000 rpm, selected results are also shown for RS2 at 5000 rpm (cf. Table 3). The values of MFB50% and the

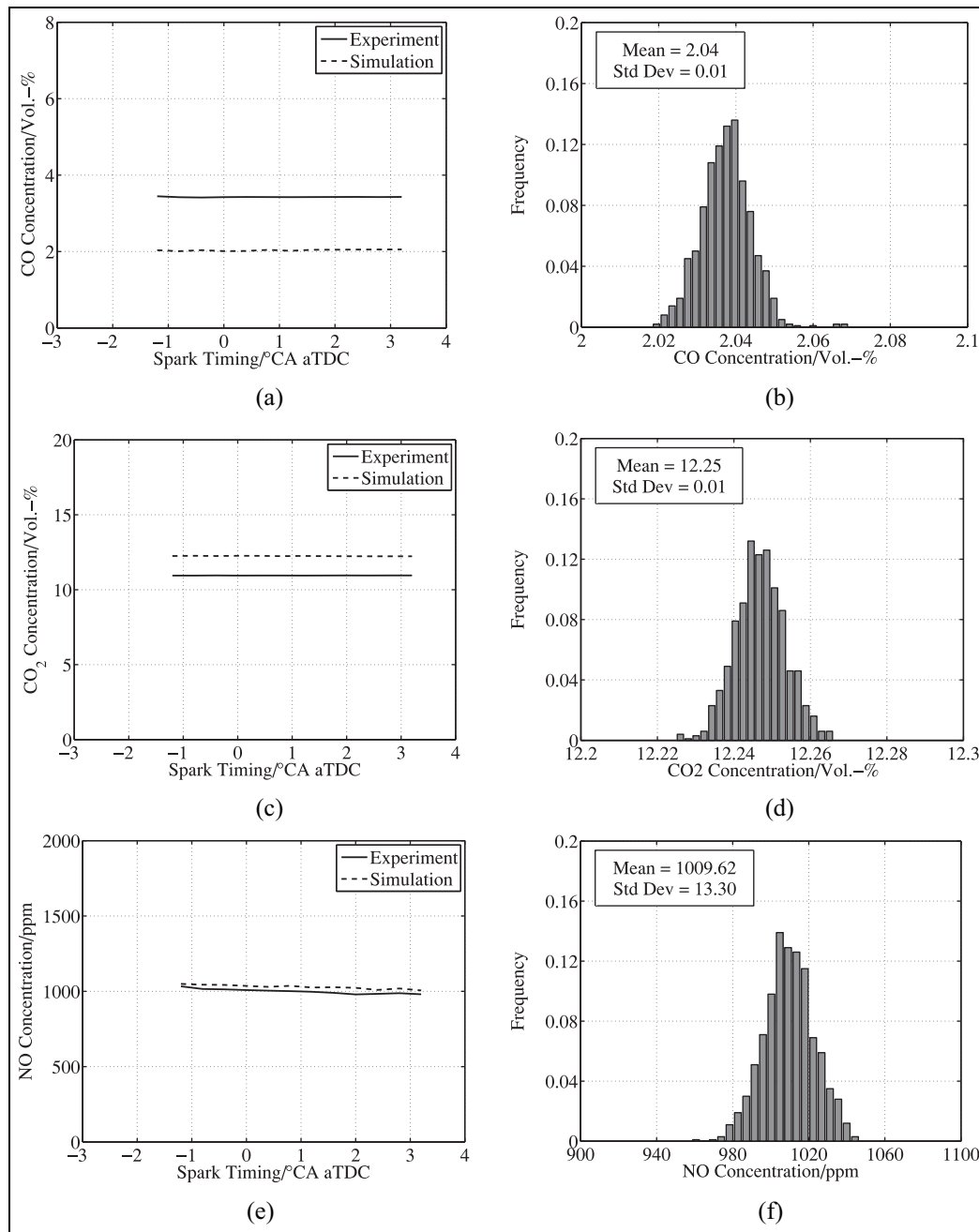


Figure 9. Validation of the residual gas model (left) and predicted cyclic variations of the residual gas composition (right): (a) experimental and predicted mean CO engine-out emissions, (b) predicted cyclic variations of the CO engine-out emissions, (c) experimental and predicted mean CO₂ engine-out emissions, (d) predicted cyclic variations of the CO₂ engine-out emissions, (e) experimental and predicted mean NO engine-out emissions, and (f) predicted cyclic variations of the NO engine-out emissions.

experimentally determined knock quantities resulting from the varied spark timings are summarized in Table 9.

For the gKIM, the Favre-averaged inverse ignition delay times are tabulated after PDF integration. The range covered and discretization of the six-dimensional look-up table are summarized in Table 10.

Following the discussions above, NO is included in exhaust gases.

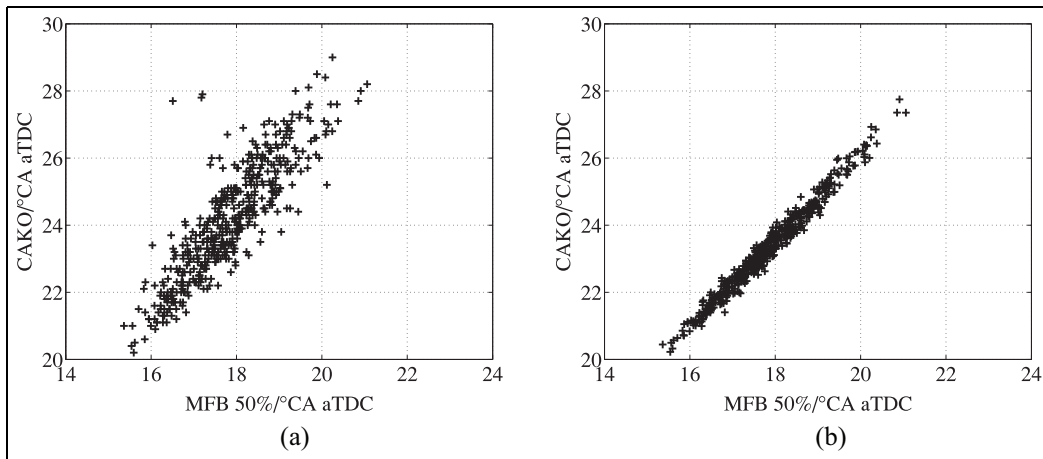
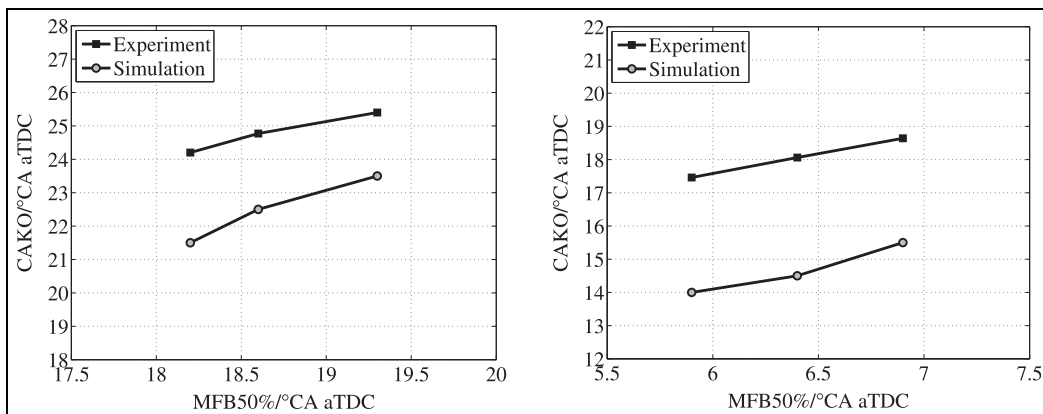
Linse et al.¹⁵ suggested that the mean CAKO can be determined by evaluating the history of the critical volume V_{I_p} . In this work, a more distinct criterion is used. The history of the critical mass m_{I_p} (cf. equation (16)) proves to be more reliable, with the peak position of m_{I_p} defining the CAKO. The benefit of the critical mass is the independence from the instantaneous cylinder volume and hence the piston position.

Table 9. Spark timing sweep based on RSI at 2000 rpm; selected points and experimental results for the knock analysis.

Case	MFB50% /°CA aTDC	CAKO /°CA aTDC	KA /bar	FKO /%
1	19.3	25.4	1.93	14.8
2	18.6	24.8	1.96	29.8
3	18.2	24.2	2.19	41.4

Table 10. Range of tabulation parameters and discretization of the look-up table.

Variable	Lower limit	Upper limit	Discretization
\bar{p}/bar	10	120	5
$T _{c=0}/K$	600	1300	25
Z	0.045	0.095	0.02
\dot{Y}_{EGR}	0.0	0.1	0.02
l_T	0.0	0.25	0.025
l_z	0.0	0.25	0.025

**Figure 10.** Multi-cycle knock simulation: (a) experimental single cycle CAKO, and (b) predicted single cycle CAKO.**Figure 11.** Comparison of the simulated mean CAKO with experimental data for the spark timing sweep: 2000 rpm (left) and 5000 rpm (right).

Moreover, it is directly related to the possible energy release of an auto-ignition.

Spark timing sweep

The comparison between the predicted and experimental CAKO is shown in Figure 11. The knock model is capable of predicting how MFB50% (spark timing) influences CAKO at 2000 and 5000 rpm. With an earlier MFB50% the mean CAKO occurs closer to TDC. However, the modeling approach predicts an earlier

overall CAKO. The deviation is about 2°CA at 2000 rpm and 3.5°CA at 5000 rpm. In general the applied model is able to predict the trends with reasonable accuracy. It should be noted that no model parameter adjustments were made based on individual operating points to improve the comparison, as this is beyond the scope of this study

Due to the particular testing program of an equal air mass flow rate at all operating points, no considerable difference in the mixture and temperature distribution is observed. Therefore, knock is mainly influenced by a

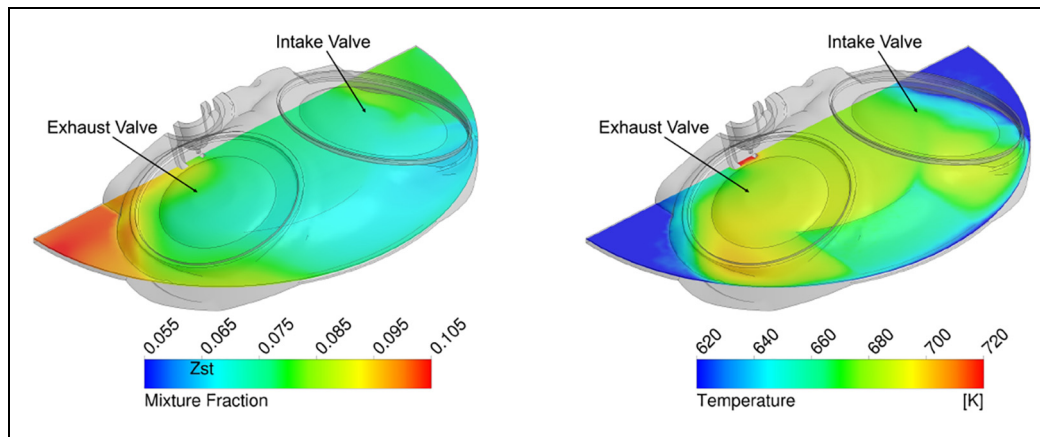


Figure 12. Case 3 of the spark timing sweep at 2000 rpm: Mixture fraction and temperature distribution at spark timing.

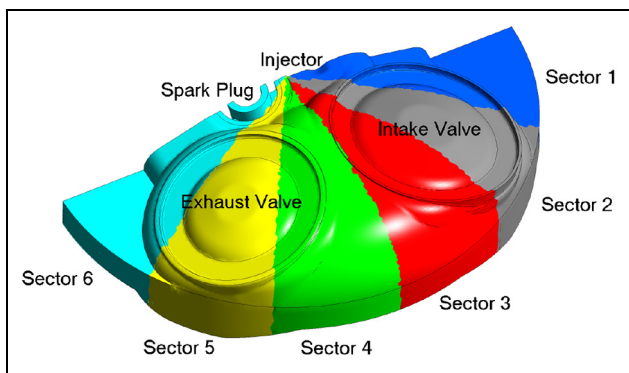


Figure 13. Definition of combustion chamber sectors.

shift in combustion progress and the associated pressure and temperature rise.

The temperature and mixture fraction distribution of Case 3 are depicted in Figure 12. The variables are evaluated on a horizontal plane at the corresponding spark timing. Fuel-rich regions (stoichiometric mixture fraction $Z_{st} = 0.065$) with high temperatures exhibit the shortest ignition delay times. Hence, auto-ignition is expected to appear first in these regions. As a result of the fuel evaporation, rich areas tend to exhibit lower temperatures. Very fuel-rich regions are located around the squish areas, especially on the exhaust side. Together with the wall heat losses, this leads to low temperatures. A fuel rich region at elevated temperature can be found below the hot exhaust valve.

Sector analysis of critical areas

These basic observations give an indication of the critical areas in the combustion chamber. To gain additional information about the location and the behavior of the critical areas, the combustion chamber is divided into six 30° sectors (cf. Figure 13). The intake side consists of Sectors 1–3 and the exhaust side is divided into

Sectors 4–6. The squish areas on the intake and exhaust side are located in Sectors 1 and 6, respectively.

In each of the six sectors, the temporal development of the following knock-related variables is evaluated and depicted in Figure 14 for Case 3.

- Critical mass m_p : Measure for the initial energy release due to auto-ignition.
- Average ignition probability of the critical cells $\bar{I}_{p, crit.}$.
- Unburned mass m_u : Mass that may be consumed by the initial auto-ignition and the following reaction.
- Average flame distance of the critical cells $\bar{\delta}_{flame}$: With a higher distance to the turbulent flame, more time is available for auto-ignition and the subsequent reactions.

The predicted mean CAKO value is shown by a vertical dotted line. The corresponding values at CAKO are highlighted by dots. Sector 5 contains the largest critical mass and ignition probability at CAKO. Sector 4 exhibits a lower critical mass compared to Sector 2 and 3, but it has a significantly higher ignition probability confirming that auto-ignition tends to happen first on the exhaust side. Moreover, the flame distance is sufficiently large, which means that the unburned mass in the critical sectors is not consumed by the propagating flame within a few CA. This can also be seen from the fact that the unburned mass in sectors 4 and 5 is twice the critical mass. This mass is consumed by the reaction wave that develops after auto-ignition.

Figure 15 shows the iso-volume of the critical cells ($I_p > 1\%$) at the instant of the predicted CAKO for Cases 1 and 3 of the spark timing sweep at 2000 rpm. The color of each computational cell indicates the local ignition probability. The knock relevant quantities in each sector at CAKO are summarized in Tables 11 and 12. Consistent with the discussion above, the regions with the highest ignition probability are located on the

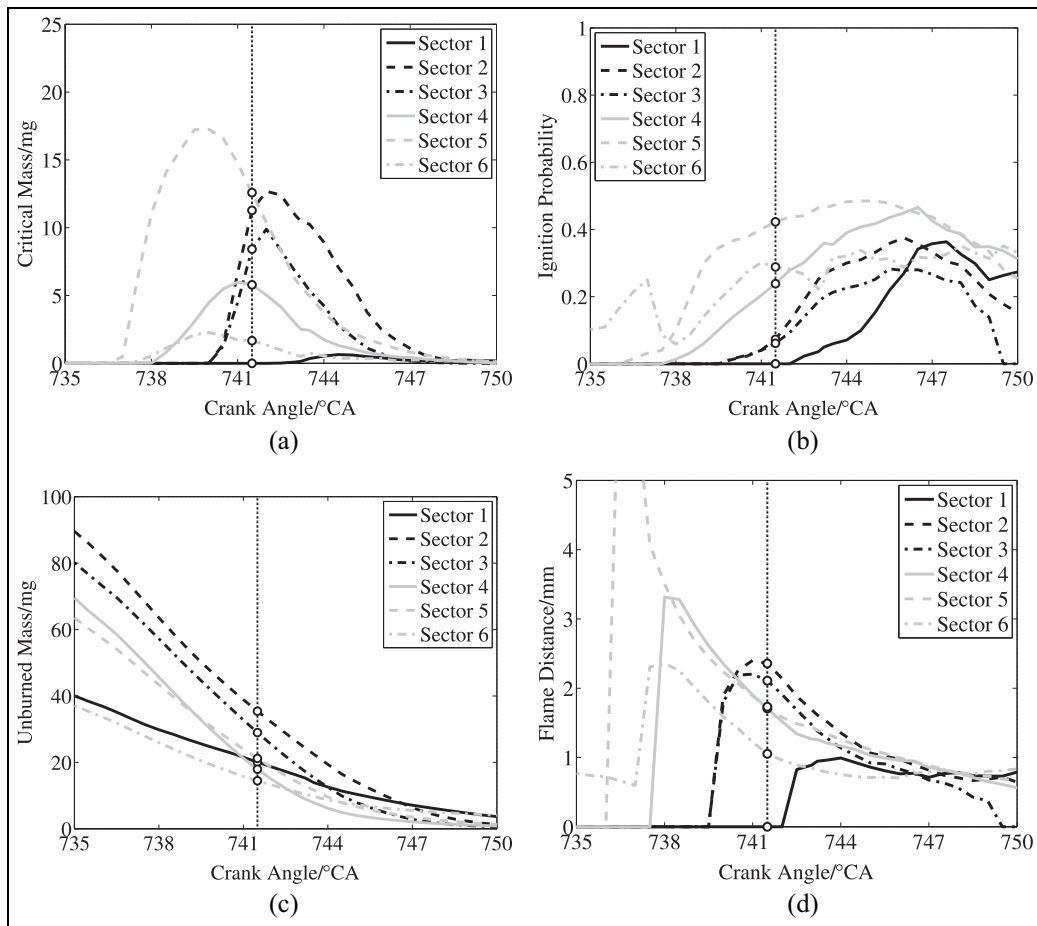


Figure 14. Evaluation of knock related quantities in each combustion chamber sector for Case 3: (a) mass of critical cells, (b) average ignition probability of critical cells, (c) unburned mass, and (d) average flame distance of critical cells.

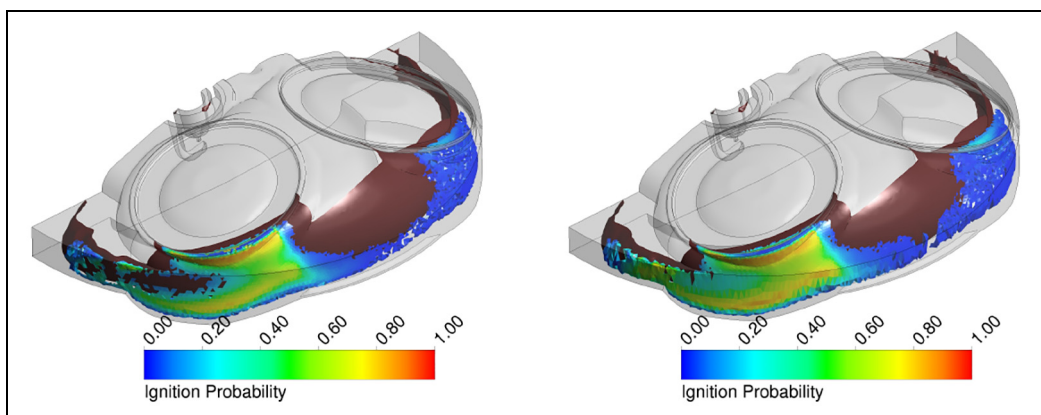


Figure 15. Ignition probability evaluated at the predicted CAKO for Case 1 (left) and Case 3 (right), spark timing sweep at 2000 rpm.

exhaust side (Sectors 4–6) and it can be seen that the locations of probable auto-ignition are hardly affected by the spark timing. Due to the high critical and unburned mass, it can be concluded that knock originates from Sector 5 in most cycles. A second region with a considerable critical mass can be found below the intake valve (Sectors 2 and 3).

The analysis of the numerical knock variables can indicate whether the experimental results are adequately described in the simulation. The comparison shows that the earlier CAKO in Case 3 leads to a larger total critical mass of 39.8 mg at CAKO (Case 1: 28.8 mg). In addition, the average ignition probability of all sectors increases slightly. Thus, Case 3 is more critical. This is

Table 11. Sector evaluation at CAKO: Case 1 of the spark timing sweep at 2000 rpm.

Sector	1	2	3	4	5	6
m_{crit}/mg	0.0	7.7	4.6	4.5	10.6	1.4
\bar{I}_p	0.00	0.05	0.05	0.21	0.39	0.21
m_u/mg	19.7	33.1	27.3	16.7	19.4	14.0
$\bar{\delta}_{flame}/mm$	0.0	2.2	2.0	1.6	1.6	1.0

Table 12. Sector evaluation at CAKO: Case 3 of the spark timing sweep at 2000 rpm.

Sector	1	2	3	4	5	6
m_{crit}/mg	0.0	11.3	8.4	5.8	12.6	1.7
\bar{I}_p	0.00	0.07	0.06	0.24	0.42	0.29
m_u/mg	20.1	35.4	29.0	17.9	21.2	14.5
$\bar{\delta}_{flame}/mm$	0.0	2.4	2.1	1.7	1.7	1.1

in qualitative agreement with the higher FKO observed in the experiments. Since the approach does not provide information whether a cycle is knocking or not, a full quantitative comparison cannot be made.

The experimental investigation confirm that higher knock amplitudes correlate with higher unburned mass fractions at CAKO. Therefore, for the higher KA of Case 3, a higher total unburned mass at CAKO would be expected. Again, the simulation results are consistent with this trend. For Case 3, a higher total unburned mass at CAKO of 138.1 mg is observed (Case 1: 130.2 mg).

Finally, Case 3 also shows a slightly higher $\bar{\delta}_{flame}$ in all sectors, meaning that more time is available for auto-ignition and subsequent reactions. This promotes the higher probability of knock.

While the 0D simulations can only predict CAKO for the mean mixture due to missing local information, the 3D CFD simulations with gKIM provide detailed information, for example, on the mixture and temperature stratification in the different combustion chamber regions and on the distance of the flame to the probable auto-ignition regions. First, it was shown for two engine speeds that the global knock trends could be predicted well. Second, a detailed analysis of the spark timing variation at the reference point RS1 showed that critical regions could be identified. These are essentially the regions near auto-ignition where sufficient unburned mixture is present.

From the comparison of the two ignition time points, it can be seen that the quantities m_{crit} , \bar{I}_p , m_u , and $\bar{\delta}_{flame}$ evaluated from the 3D CFD are consistent with the experimental trends.

Conclusions

Knocking combustion was studied experimentally and with 0D and 3D simulation approaches both of which use detailed chemistry. The basis was an extensive experimental data base for two different engine speeds.

Variations of intake pressure, intake temperature and air-fuel ratio were carried out. For each operating point, a spark timing sweep was conducted. In order not to change the fluid mechanical conditions and thus to ensure good comparability, the air mass flow (load) was kept the same. The main findings can be summarized as follows.

- The experimental results showed that knock is strongly affected by the combustion progress. An earlier MFB50% (crank angle at which 50% of the cylinder mass is burned) was shown to lead to a higher frequency of knock onset (FKO) and an earlier crank angle at knock onset (CAKO) and promote the occurrence of higher knock amplitudes. Analysis of the individual cycles indicated that high knock amplitudes may be correlated to higher unburned mass fractions at CAKO. However, only a certain amount of the unburned mass fraction at CAKO is consumed by auto-ignition.
- NO contained in the exhaust gases must be considered when predicting auto-ignition/CAKO despite very low residual gas fractions in the preceding cycle. This was confirmed for all operating points. A zero-dimensional knock modeling approach was applied to the averaged engine cycles of all measured operating points. It was demonstrated that neglecting NO leads to a significantly delayed auto-ignition and reduces the overall accuracy of the modeling approach. NO was also included in the detailed chemistry approach in 3D CFD.
- It was demonstrated that the implemented zero-dimensional knock model is able to predict the mean crank angle at knock onset under various operating conditions with reasonable accuracy. These findings are based on the calculation of the average cycle.
- The evaluation of the experimental results revealed that considerable cycle-to-cycle knock variations

occur, which cannot be completely explained by the cyclic variability of the combustion. Hence, the 0D knock model was applied on a multi-cycle basis to investigate possible causes. In this work 1000 cycles were considered for each studied operation point. The overall trend was captured well by the simulation. However, although all available information was considered, the model was not able to reproduce the considerable fluctuations in CAKO at a constant MFB50%. This indicates that knocking is substantially influenced by local effects.

- To investigate these local effects on the formation of knocking combustion, a modified generalized knock integral method (gKIM) was proposed and used in 3D CFD simulations. Detailed chemical kinetics were applied and the impact of temperature and mixture fraction fluctuations was taken into account. The predicted CAKO was validated against the experimental data. The results showed that the modeling approach is able to capture the trend for varied operating parameters. Critical areas in the combustion chamber were identified. The evaluation of the knock-related quantities in the six combustion chamber sectors provided additional information, which helped to characterize and classify the critical areas.
- With respect to the 3D CFD investigation, it should be noted, that the RANS analysis is limited due to its averaging nature. Although fluctuations are taken into account in the gKIM, it does not fully describe the stochastic nature of knocking combustion which occurs in single cycles.

Future work

Recently published LES studies for a few selected operating points show very promising results to overcome the limitations of RANS simulations. Future LES studies should aim to investigate comprehensive data sets like the ones presented here. In addition, effects other than mixture and temperature inhomogeneities, such as boundary layer related phenomena, should be investigated. Experimental studies should aim to include further parameter variations, for example, with respect to the injection process.

Acknowledgement

The work of Magnus Kircher is supported by the Graduate School CE within the Centre for Computational Engineering at Technical University Darmstadt.



Declaration of conflicting interests

The author(s) declared no potential conflicts of interest with respect to the research, authorship, and/or publication of this article.

Funding

The author(s) disclosed receipt of the following financial support for the research, authorship, and/or publication of this article: Funded by the Deutsche Forschungsgemeinschaft (DFG, German Research Foundation) – Project no. 423158633.

ORCID iDs

Magnus Kircher  <https://orcid.org/0000-0001-9006-8954>
Christian Hasse  <https://orcid.org/0000-0001-9333-0911>

References

1. Kalghatgi G. Knock onset, knock intensity, superknock and preignition in spark ignition engines. *Int J Engine Res* 2018; 19(1): 7–20.
2. Wang Z, Liu H and Reitz RD. Knocking combustion in spark-ignition engines. *Prog Energy Combust Sci* 2017; 61: 78–112.
3. Ricardo H. *The internal combustion engine vol II: high-speed engines*. Vol. 2. Glasgow and Bombay: Blackie and Son Limited, 1923.
4. Heywood JB. *Internal combustion engine fundamentals*. Vol. 26. New York: McGraw-Hill, 1988.
5. Miller C. *Relation between spark-ignition engine knock, detonation waves, and autoignition as shown by high-speed photography*. Technical Report 855, Washington: NACA, 1946.
6. König G, Maly RR, Bradley D, Lau AKC and Sheppard CGW. Role of exothermic centres on knock initiation and knock damage. *SAE Technical Paper* 902136, 1990.
7. Spicher U, Kröger H and Ganser J. Detection of knocking combustion using simultaneously high-speed Schlieren cinematography and multi optical fiber technique. *SAE Technical Paper* 912312, 1991.
8. Zeldovich Y. Regime classification of an exothermic reaction with nonuniform initial conditions. *Combust Flame* 1980; 39(2): 211–214.
9. Bradley D, Morley C, Gu XJ and Emerson DR. Amplified pressure waves during autoignition: relevance to CAI engines. *SAE Technical Paper* 2002-01-2868, 2002.
10. Bradley D and Kalghatgi GT. Influence of autoignition delay time characteristics of different fuels on pressure waves and knock in reciprocating engines. *Combust Flame* 2009; 156(12): 2307–2318.
11. Kalghatgi GT and Bradley D. Pre-ignition and ‘superknock’ in turbo-charged spark-ignition engines. *Int J Engine Res* 2012; 13: 399–414.
12. Peters N, Kerschgens B and Paczko G. Super-knock prediction using a refined theory of turbulence. *SAE Int J Engines* 2013; 6(2): 953–967.
13. Wang Z, He X, Liu H, Qi Y, Zhang P and Wang J. Initiation of detonation in iso-octane/air mixture under high pressure and temperature condition in closed cylinder. In *Proceedings of the 25th International Colloquium on the Dynamics of Explosions and Reactive Systems, ICDERS*, Paper 090, 2015, pp. 1–7.
14. Meng LV, Yun LI, Xiaoming HU, Yongchen LIU and Chang LV. Super-knock suppression using split injection in a turbo-charged GDI engine. *MATEC Web Conf* 2016; 40: 02011.1–3.

15. Linse D, Kleemann A and Hasse C. Probability density function approach coupled with detailed chemical kinetics for the prediction of knock in turbocharged direct injection spark ignition engines. *Combust Flame* 2014; 161(4): 997–1014.
16. D'Adamo A, Breda S, Fontanesi S and Cantore G. A RANS-based CFD model to predict the statistical occurrence of knock in spark-ignition engines. *SAE Int J Engines* 2016; 9(1): 618–630.
17. Netzer C, Seidel L, Pasternak M, et al. Three-dimensional computational fluid dynamics engine knock prediction and evaluation based on detailed chemistry and detonation theory. *Int J Engine Res* 2018; 19(1): 33–44.
18. d'Adamo A, Breda S, Berni F and Fontanesi S. The potential of statistical RANS to predict knock tendency: comparison with LES and experiments on a spark-ignition engine. *Appl Energy* 2019; 249: 126–142.
19. Fontanesi S, d'Adamo A and Rutland CJ. Large-Eddy simulation analysis of spark configuration effect on cycle-to-cycle variability of combustion and knock. *Int J Engine Res* 2015; 16(3): 403–418.
20. Robert A, Richard S, Colin O, Martinez L and De Francqueville L. LES prediction and analysis of knocking combustion in a spark ignition engine. *Proc Combust Inst* 2015; 35(3): 2941–2948.
21. Robert A, Richard S, Colin O and Poinso T. LES study of deflagration to detonation mechanisms in a downsized spark ignition engine. *Combust Flame* 2015; 162(7): 2788–2807.
22. Robert A, Truffin K, Iafrate N, Jay S, Colin O and Angelberger C. Large-eddy simulation analysis of knock in a direct injection spark ignition engine. *Int J Engine Res* 2019; 20(7): 765–776.
23. Krastev VK, d'Adamo A, Berni F and Fontanesi S. Validation of a zonal hybrid URANS/LES turbulence modeling method for multi-cycle engine flow simulation. *Int J Engine Res* 2020; 21(4): 632–648.
24. Chun KM. *Characterization of knock and prediction of its onset in a spark-ignition engine*. PhD Thesis, Massachusetts Institute of Technology, Cambridge, MA, 1988.
25. Lindemann M and Funk T. Einfluss verschiedener Filterverfahren auf die Generierung druckbasierter Klopfmerkmale. In: Fischer M (ed.) *Klopfregelung für Ottomotoren, Haus der Technik Fachbuch*. Vol. 31. Expert-Verlag GmbH: Renningen, 2004, pp.139–147.
26. Chiriac R, Radu B, Apostolescu N and Fuioreescu D. An investigation of knock in a spark ignition engine using LPG. *SAE Technical Paper* 2005-24-027, 2005.
27. Fischer M, Günther M, Röpke K, Lindemann M and Placzek R. Klopfkennung im Ottomotor: Neue Tools und Methoden in der Serienentwicklung. *MTZ Motor-technische Zeitschrift* 2003; 64: 186–194.
28. Christiner P, Chmela F, Dimitrov D, Pirker G and Wimmer A. Potenziale null- und dreidimensionaler Simulationsmethoden zur Klopfvorhersage. In Günther M (ed.) *Ottomotorisches Klopfen Irreguläre Verbrennung/Knocking Gasol. Engines – Irregular Combustion*. Expert-Verlag GmbH.
29. Schüle H, Stutika M and Schneider W. Zylinderdruckbasierte Klopfkennung: Funktionsansätze, Umsetzung in der Motorsteuerung, Ergebnisse am Motorenprüfstand. In: Günther M (ed.) *Ottomotorisches Klopfen – Irreguläre Verbrennung/Knocking at Gasoline Engines – Irregular Combustion*. Expert-Verlag GmbH, Berlin, 2010, 321–343.
30. Leppard WR. Individual-Cylinder knock occurrence and intensity in multicylinder engines. *SAE Technical Paper* 820074, 1982.
31. Cowart JS, Haghgoie M, Newman CE, Davis GC, Pitz WJ and Westbrook CK. The intensity of knock in an internal combustion engine: an experimental and modeling study. *SAE Technical Paper* 922327, 1992.
32. Lämmle C. *Numerical and experimental study of flame propagation and knock in a compressed natural gas engine*. PhD Thesis, ETH Zürich, Zürich, Switzerland, 2005.
33. Soyulu S. Prediction of knock limited operating conditions of a natural gas engine. *Energy Convers Manag* 2005; 46(1): 121–138.
34. Bade Shrestha SO and Karim GA. A predictive model for gas fueled spark ignition engine applications. *SAE Technical Paper* 1999-01-3482, 1999.
35. Liu Z and Chen R. A zero-dimensional combustion model with reduced kinetics for SI engine knock simulation. *Combust Sci Technol* 2009; 181(6): 828–852.
36. Livengood JC and Wu PC. Correlation of autoignition phenomena in internal combustion engines and rapid compression machines. *Symp. Combust* 1955; 5(1): 347–356.
37. Linse D. *Modeling and Simulation of Knock and Nitric Oxide Emissions in Turbocharged Direct Injection Spark Ignition Engines*. PhD Thesis, TU Bergakademie Freiberg, 2013.
38. Kato M and Launder BE. *The modelling of turbulent flow around stationary and vibrating cylinders*. Kyoto, Japan, 1993.
39. Keller-Sornig P. *Berechnung der turbulenten Flammenausbreitung bei der ottomotorischen Verbrennung mit einem Flamelet-Modell*. PhD Thesis, RWTH Aachen, 1997.
40. Toninel S, Forkel H, Frank T, Durst B, Hasse C and Linse D. Implementation and validation of the G-equation model coupled with flamelet libraries for simulating premixed combustion in I.C. Engines. *SAE Technical Paper* 2009-01-0709, 2009.
41. Stach T, Schlerfer J and Vorbach M. New generation multi-hole fuel injector for direct-injection SI engines – optimization of spray characteristics by means of adapted injector layout and multiple injection. *SAE Technical Paper* 2007-01-1404, 2007.
42. Lafossas FA, Castagne M, Dumas JP and Henriot S. Development and validation of a knock model in spark ignition engines using a CFD code. *SAE Technical Paper* 2002-01-2701, 2002.
43. Kleemann AP, Menegazzi P, Henriot S and Marchal A. Numerical study on knock for an SI engine by thermally coupling combustion chamber and cooling circuit simulations. *SAE Technical Paper* 2003-01-0563, 2003.
44. Teraji A, Tsuda T, Noda T, Kubo M and Itoh T. Development of a three-dimensional knock simulation method incorporating a high-accuracy flame propagation model. *Int J Engine Res* 2005; 6(1): 73–83.
45. Christiner P, Jauk T, Kogler G and Wimmer A. Methodik zur Verbesserung des Klopfverhaltens von Gasmotoren mit offenem Brennraum. In *9. Internationales Symposium für Verbrennungsdiagnostik*–Baden Baden, Deutschland, 8–9 June 2010.
46. Jaworski P, Priesching P, Teodorczyk A and Bandel W. Validation of the numerical simulation of Iso-octane

- auto-ignition delay time in rapid compression machine with the use of ECFM-3Z (extended coherent flame model – 3 zones) combustion model against experimental data. *Combustion* 2010; 30(1): 1–14.
47. Lee Y, Pae S, Min K and Kim ES. Prediction of knock onset and the autoignition site in spark-ignition engines. *Proc IMechE, Part D: J Automobile Engineering* 2000; 214: 751–763.
 48. Choi H, Hwang SH, Lee J and Min K. 3-dimensional simulation of knock in a heavy-duty LPG engine. *SAE Technical Paper* 2002-01-2700, 2002.
 49. Liang L, Reitz RD, Iyer CO and Yi J. Modeling knock in spark-ignition engines using a G-equation combustion model incorporating detailed chemical kinetics. *SAE Technical Paper* 2007-01-0165, 2007.
 50. Eckert P, Kong SC and Reitz RD. Modeling autoignition and engine knock under spark ignition conditions. *SAE Technical Paper* 2003-01-0011, 2003.
 51. Liberman MA, Ivanov MF, Peil OE, Valiev DM and Eriksson LE. Numerical modeling of the propagating flame and knock occurrence in spark-ignition engines. *Combust Sci Technol* 2004; 177(1): 151–182.
 52. Kawabata Y, Sakonji T and Amano T. The effect of NOx on knock in spark-ignition engines. *SAE Technical Paper* 1999-01-0572, 1999.
 53. Stenlås O, Gogan A, Egnell R, Sundén B and Mauss F. The influence of nitric oxide on the occurrence of auto-ignition in the end gas of spark ignition engines. *SAE Technical Paper* 2002-01-2699, 2002.
 54. Frassoldati A, Faravelli T and Ranzi E. Kinetic modeling of the interactions between NO and hydrocarbons at high temperature. *Combust Flame* 2003; 135(1–2): 97–112.
 55. Burluka AA, Liu K, Sheppard CG, Smallbone AJ and Woolley R. The influence of simulated residual and NO concentrations on knock onset for PRFs and gasolines. *SAE Technical Paper* 2004-01-2998, 2004.
 56. Moréac G, Dagaut P, Roesler JF and Cathonnet M. Nitric oxide interactions with hydrocarbon oxidation in a jet-stirred reactor at 10 atm. *Combust Flame* 2006; 145(3): 512–520.
 57. Dubreuil A, Foucher F, Mounaïm-Rousselle C, Dayma G and Dagaut P. HCCI combustion: effect of NO in EGR. *Proc Combust Inst* 2007; 31: 2879–2886.
 58. Machrafi H, Cavadias S and Guibert P. An experimental and numerical investigation on the influence of external gas recirculation on the HCCI autoignition process in an engine: thermal, diluting, and chemical effects. *Combust Flame* 2008; 155(3): 476–489.
 59. Anderlohr J, Bounaceur R, Pires Da Cruz A and Battin-Leclerc F. Modeling of autoignition and NO sensitization for the oxidation of IC engine surrogate fuels. *Combust Flame* 2009; 156(2): 505–521.
 60. Anderlohr JM, Piperel A, Pires da Cruz A, et al. Influence of EGR compounds on the oxidation of an HCCI-diesel surrogate. *Proc Combust Inst* 2009; 32(2): 2851–2859.
 61. Hoffmeyer H, Montefrancesco E, Beck L, Willand J, Ziebart F and Mauss F. CARE – CAlytic reformed exhaust gases in turbocharged DISI-engines. *SAE Technical Paper* 2009-01-0503, 2009.